IEEE Photonics Journal
An IEEE Photonics Society Publication

Open Access

Microfiber-Based Inline Mach–Zehnder Interferometer for Dual-Parameter Measurement

Volume 7, Number 2, April 2015

Haipeng Luo
Qizhen Sun
Zhilin Xu
Weihua Jia
Deming Liu
Lin Zhang

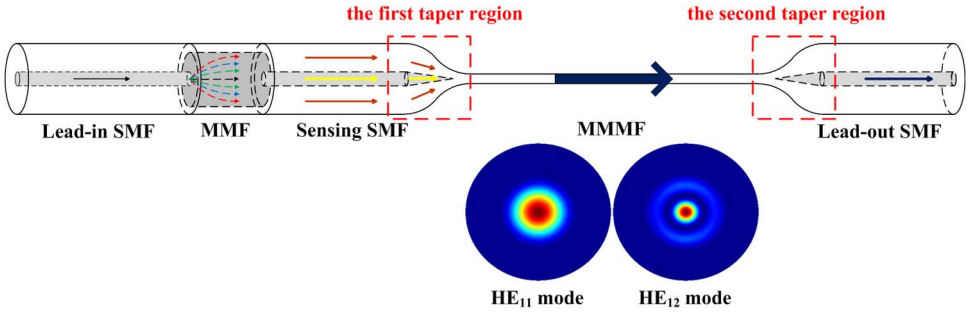

DOI: 10.1109/JPHOT.2015.2395133
1943-0655

IEEE photonics SOCIETY

IEEE

Microfiber-Based Inline Mach–Zehnder Interferometer for Dual-Parameter Measurement

Haipeng Luo, Qizhen Sun, Zhilin Xu, Weihua Jia, Deming Liu, and Lin Zhang

National Engineering Laboratory for Next Generation Internet Access System, School of Optical and Electronic Information, Huazhong University of Science and Technology, Wuhan 430074, China
Aston Institute of Photonic Technologies, Aston University, Birmingham, B4 7ET, U. K.

DOI: 10.1109/JPHOT.2015.2395133

Manuscript received December 3, 2014; revised January 5, 2015; accepted January 17, 2015. Date of publication February 16, 2015; date of current version March 16, 2015. This work was supported in part by the National Natural Science Foundation of China under Grant 61275004 and Grant 61290315 and in part by the European Commission's Marie Curie International Incoming Fellowship under Grant 328263. Corresponding author: Q. Sun (e-mail: qzsun@mail.hust.edu.cn).

Abstract: An approach to realizing simultaneous measurement of refractive index (RI) and temperature based on a microfiber-based dual inline Mach–Zehnder interferometer (MZI) is proposed and demonstrated. Due to different interference mechanisms, as one interference between the core mode and the lower order cladding mode in the sensing single-mode fiber and the other interference between the fundamental mode and the high-order mode in the multimode microfiber, the former interferometer achieves RI sensitivity of −23.67 nm/RIU and temperature sensitivity of 81.2 pm/oC, whereas those of the latter are 3820.23 nm/RIU, and −465.7 pm/oC, respectively. The large sensitivity differences can provide a more accurate demodulation of RI and temperature. The sensor is featured with multiparameters measurement, compact structure, high sensitivity, low cost, and easy fabrication.

Index Terms: Sensors, subwavelength structures, refractive index, temperature.

1. Introduction

Micro/nanofiber (MNF) has been widely used in grating [1], resonator [2] and sensor [3] in the past few years, due to its unique and promising optical properties of low transmission loss, large evanescent field, high nonlinear effect, and tight optical confinement. Among these merits, large evanescent field make MNF to have the application prospect in chemical and biomedical areas. During these fields, refractive index (RI) and temperature are the two most important parameters owning to direct reflection of physical properties of materials. Recently, many investigation have been done for RI or temperature sensing, including optical microfiber mode interferometer [4], D-shaped microfiber [5], and microfiber-based Mach-Zehnder interferometer (MZI) [6] for RI sensing, and multimode fiber tip [7], silica/polymer microfiber knot resonators (SMKR/PMKR) [8], and isopropanol-sealed optical microfiber taper (OMT) [9] for constructing temperature sensor. However, as we all known, temperature will strongly influence the RI of solution due to a large thermo-optic coefficient, therefore, distinguish them effectively during measurement is extremely important.

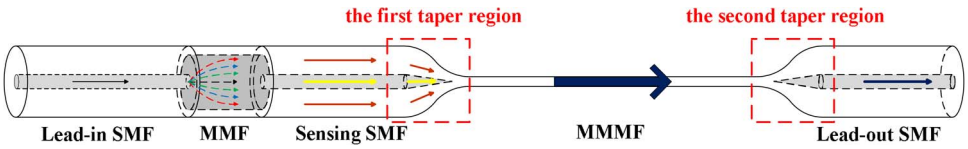

Fig. 1. Structure of the sensing element.

Over the past few years, significant efforts based on microfiber have been devoted to the development of simultaneous measurement of RI and temperature, such as the microfiber Fabry-Perot interferometer (MFPI) [10] and our previous work of multimode microfiber (MMMF) based dual MZI [11]. Other fiber structure like microfiber Bragg gratings (mFBGs) [12], [13] are proposed for temperature independent RI sensing, which also have the ability of simultaneous dual-parameters measurement. However, the MMMF based dual MZI has complex configuration and less stability due to the natural defect of two arms MZI setup, while the MFPI and mFBGs require UV laser photolithograph FBG, which increases equipment cost and manufacturing difficulty.

In this paper, we present a compact dual in-line MZI by tapering the designated region of fiber structure into micrometer size, then forming (single-mode fiber)-(multimode fiber)-(single-mode fiber)-(multimode microfiber)-(single mode fiber) (SMSMS) structure, providing simultaneous measurement of RI and temperature with high sensitivities. The dual in-line MZI is composed of one in-line MZI between the core mode and the cladding mode in the SSMF and the other in-line MZI between the fundamental mode and the high order mode in the MMMF. The former MZI provides an interference envelope with a large free spectrum range (FSR) while the latter MZI generates a dense interference fringe with a small FSR and modulated by the interference envelope. Due to different interference mechanisms of the two MZIs, the specific interference fringes have different responses to the external variation and, consequently, offer the possibility of dual-parameters measurement.

2. Schematic Diagram and Theoretical Simulation

2.1. Structure of the Sensing Element

The structure of the sensing element is shown as Fig. 1, which is fabricated with the following steps. First, a section of single mode fiber (SMF) is spliced with the multimode fiber (MMF) possessing core and cladding diameter of 100/125 Km and the spliced point named the first spliced point is marked. Secondly, the MMF is cut off at the point which is 8 mm away from the first spliced point to form single-mode fiber-multimode fiber (SM) structure. Thirdly, the SM fiber structure is spliced again with SMF to form single-mode-multimode-single-mode (SMS) fiber structure, and the spliced point is named as the second spliced point. Lastly, the heated region with 15 mm away from the second spliced point is selected and tapered down into micrometer size by hydrogen flame, and thus the tapered SMF turns into three sections including the sensing SMF, MMMF, and lead-out SMF. In this way, the SMSMS fiber structure is constructed.

2.2. Working Principle of the Sensing Element

When the light transmits from the lead-in SMF into the MMF and then the SSMF, at the spliced point between MMF and SSMF, optical power is partly coupled into the cladding modes of the SSMF and partly remained in the core mode on account of the mode field mismatch. Then the cladding and core modes are collected by the taper region, and interference is generated due to optical path difference. It is confirmed that the interference in the SSMF is dominated by the low-order cladding mode and the core mode [14]. Owing to the fact that both modes propagate in the same fiber, the interference is an in-line MZI. Consequently, when the light transmits from the taper region into the MMMF with waist diameter less than 12 7 μm, two main modes i.e., HE_{11} mode and HE_{12} mode are excited [15], [16], and then, the other in-line MZI between the two guided modes are produced at the same time. As a result, the transmission spectrum containing

two MZIs are guided out through the lead-out SMF and analyzed by the signal processing system. One highlight of the SMSMS fiber structure should be pointed out that the two in-line MZIs are independent to each other, which provides favorable property of simple demodulation of each MZI variation separately from the transmission spectrum.

2.3. Simulation of RI and Temperature Sensitivities

The resonant dip λ_p in the interference fringe generated by the in-line MZI between the core mode and the low-order cladding mode in SMMF can be expressed as

$$(n_0 - n')L_0 = \Delta n_{eff0} L_0 = \left(p + \frac{1}{2}\right)\lambda_p \tag{1}$$

where n_0 and n' are the effective RI of the core mode and the low-order cladding mode, respectively. L_0 is the length of SMMF, Δn_{eff0} represents the effective RI difference between the two modes, and p is a positive integer.

It is obvious that dip λ_p will shift to short wavelength along with surrounding RI (SRI) increasing [14], [17], because Δn_{eff0} will decrease as n' increases which is subjected to SRI [14]. Meanwhile, the temperature sensitivity of dip λ_p is usually around dozens of picometer per Celsius [18], [19], which is much higher than that of fiber Bragg grating (FBG), due to the significantly different thermo-optic coefficients between the core and the cladding in the SSMF [19].

For the other in-line MZI between the two guided modes in the MMMF, its resonant dip λ_q can be described as

$$(n_1 - n_2)L = \Delta n_{eff} L = \left(q + \frac{1}{2}\right)\lambda_q \tag{2}$$

where n_1 and n_2 are the effective RI of HE_{11} mode, and HE_{12} mode in MMMF L represents the length of MMMF, Δn_{eff} is the effective RI difference between the two modes, and q is a positive integer.

MMMFs always achieve high RI sensitivity [4], [11] and temperature sensitivity [9], [11]; however, systematic prediction of the sensing performance has not been done to the best of our knowledge, especially temperature sensing. In this part, we focused on theoretical analysis of RI sensitivities as a function of MMMF diameter and SRI as well as temperature sensitivities subjected to the MMMF diameter and thermo-optic efficient of surrounding solution.

For a MMMF with diameter of several micrometers, the MMMF is considered to be a uniform medium with the same material of the SMF cladding. According to the circular cross-section optical waveguide theory, the propagation constants i.e., β_1 and β_2, respectively, corresponding to HE_{11} mode and HE_{12} mode supported by MMMF, are the two most important parameters, and can be calculated from the eigenvalue equations [20]. The relationship between the propagation constant β and the effective RI of the eigenvalue mode n_{eff} is $n_{eff} = \lambda\beta/2\pi$, where λ is the light wavelength.

Then, RI sensitivity of dip λ_q i.e., S_{RI} can be calculated through the following equation by transforming (2) [21]:

$$S_{RI} = \frac{d\lambda_q}{dn} = \frac{\lambda_q \frac{\partial(\Delta n_{eff})}{\partial n}}{\Delta n_{eff} - \lambda_q \frac{\partial(\Delta n_{eff})}{\partial \lambda_q}} = \frac{\lambda_q}{G}\frac{\partial(\Delta n_{eff})}{\partial n} \tag{3}$$

where $G = \Delta n_{eff} - \lambda_q \times \partial(\Delta n_{eff})/\partial\lambda$ is the group effective RI difference between HE_{11} mode and HE_{12} mode in MMMF. To investigate the methods to improve the RI sensitivity, we analyzed the key impact parameters like diameter of MMMF, and SRI. These two parameters dominate Δn_{eff}, and thus affect the RI sensitivity. Assuming that the RI of the fiber material is 1.444 at wavelength of 1550 nm, we calculate the RI sensitivities of MMMF with diameter ranging from 5 μm to 12 μm at SRI of 1.3310, 1.3410, and 1.3510 exhibited in Fig. 2(a). It clearly shows that the sensitivities will be enhanced along with diameter of MMMF decreasing at a certain

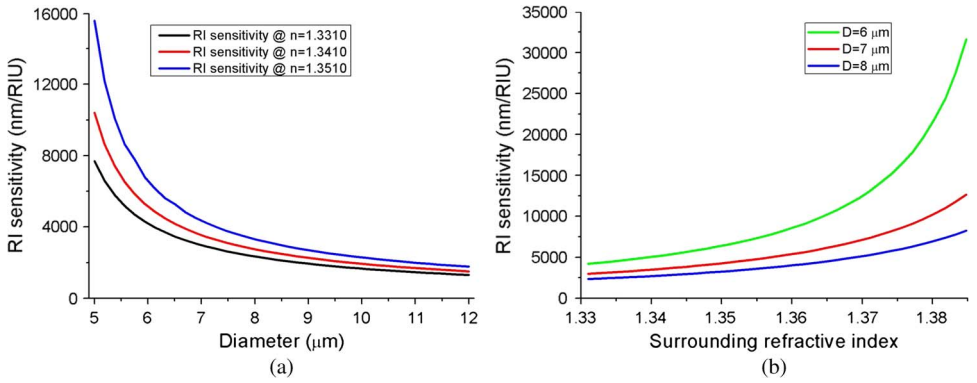

Fig. 2. (a) Calculated RI sensitivity of MMMF based in-line MZI with different diameters. (b) Simulated RI sensitivities within the RI range of 1.3310–1.3850 at certain fiber diameters.

SRI. For example, at SRI of 1.3510, the RI sensitivity will be high as 15560 nm/RIU with a diameter of 5 μm, which is much larger than the sensitivity of only 1770.1 nm/RIU at diameter of 12 μm. Fig. 2(b) demonstrates the relationship between RI sensitivity and SRI, which indicates that the RI sensitivity of MMMF is over than 2300 nm/RIU within a large SRI variation scope and much higher RI sensitivity can be achieved with a relatively larger SRI. For instance, for MMMF with a diameter of 6 μm, the RI sensitivity will reach 31 598 nm/RIU at SRI of 1.3848, while it will decrease to 4192 nm/RIU when SRI is 1.3310.

The working principle of temperature sensing is similar to the RI sensing, as the resonant wavelength shift is also caused by Δn_{eff} variation when temperature changes. Temperature sensitivity S_T calculation equation (4) is actually transformed from (3), where variable temperature i.e. T is used to replace variable RI i.e., n.

$$S_T = \frac{d\lambda_q}{dT} = \frac{\lambda_q \frac{\partial(\Delta n_{eff})}{\partial T}}{\Delta n_{eff} - \lambda_q \frac{\partial(\Delta n_{eff})}{\partial \lambda_q}} = \frac{\lambda_q}{G} \frac{\partial(\Delta n_{eff})}{\partial T}. \tag{4}$$

In this equation, Δn_{eff} is determined by temperature through thermo-optic effect of the fiber and that of solution When the temperature changes, the RI of MMMF correspondingly varies with thermo-optic efficient of 0.68×10^{-5} RIU/°C as well as that of solution will also change. Assuming the surrounding mediums are sucrose solution, glycerin solution, and isopropanol with thermo-optic coefficient of -1×10^{-4} RIU/°C, -3.5×10^{-4} RIU/°C [22], and -4.5×10^{-4} RIU/°C [9], respectively, the simulated temperature sensitivities of MMMF with different diameters at SRI of 1.3631 are presented in Fig. 3(a), which indicates that the temperature sensitivity is a negative value. More information we can get from the graph is that temperature sensitivity will be much improved by employing the MMMF with a smaller diameter. For example, we can seal the MMMF in isopropanol for only temperature sensing, and the sensitivity nearly -16 nm/°C can be obtained at the diameter of 5 Km while the sensitivity is limited at -1.04 nm/°C at the diameter of 12 Km. Moreover, Fig. 3(b) shows the temperature sensitivities as a function of thermo-optic coefficient, which illustrates that the temperature sensitivity is almost linearly proportional to the thermo-optic coefficient and higher thermo-optic efficient brings higher temperature sensitivity.

3. Experimental Results

Fig. 4(a) exhibits the schematic diagram of the experimental setup, which contains a circulator, an interrogation system (Micron Optics, Inc., sm125-500), including a broadband light source ranging from 1510 nm to 1590 nm and an optical spectrum analysis with wavelength scanning interval of 5 pm and accuracy of 1 pm, and a signal processing system, which is used to analyze and demodulate the transmission spectrum. The sensing element is the SMSMS fiber

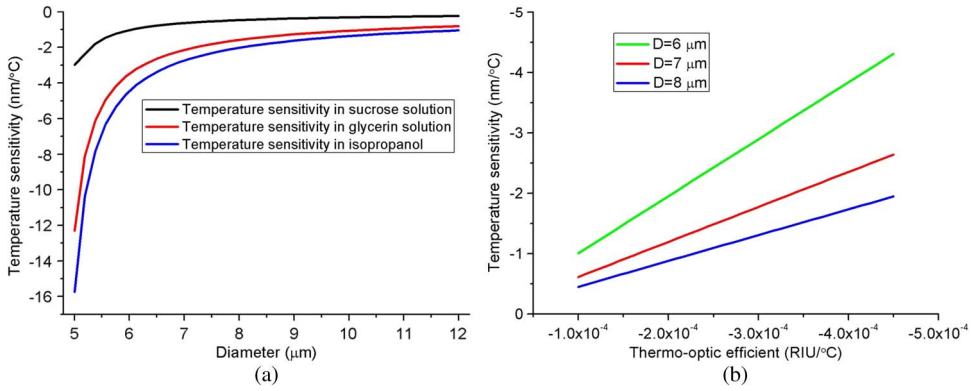

Fig. 3. (a) Calculated temperature sensitivity of MMMF based in-line MZI with different diameters at n = 1.3631. (b) Simulated temperature sensitivities within the solution thermo-optic efficient range from -1×10^{-4} to -4.5×10^{-4} at certain fiber diameters.

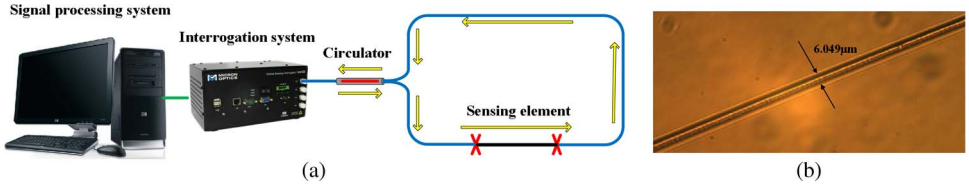

Fig. 4. (a) Schematic diagram of the experiment. (b) Microscope image of MMMF.

structure, and the lengths of SSMF and MMMF are selected to be 15 mm and 26 mm, respectively. Microscope image of the MMMF is shown in Fig. 4(b). The length of the first taper region and the second taper region are around 4.7 mm and 5.2 mm, respectively, and the uniform waist section has a length of 16.1 mm, and the diameter is about 6.049 Km supporting multimode transmission.

The RI experiment is implemented by immersing the sensing element in different concentrations of sucrose solution. Typical transmission spectrums with external RI of 1.3320 and 1.3325 are exhibited in Fig. 5. As we can see, the spectrum contains an interference envelope with large FSR as well as a dense interference fringe with amplitude modulation, corresponding to the in-line MZIs in SSMF and MMMF, respectively. The envelope dip cannot be directly obtained from the wide band and modulated transmission spectrum, therefore, special data processing steps are taken as follows: firstly, we choose a section of transmission spectrum which contains the envelop dip as the sample; second, we directly get the wavelength corresponding to the minimum power within the sample and record it; third, we use Guass function to fit the transmission spectrum within 24 nm wavelength range on the center of the recorded wavelength; finally, we calculate the dip from the fitting function as dip1. The insert picture depicts the enlarged spectrums, with wavelength ranging from 1548 to 1557.5 nm, which clearly shows that the FSR of the dense spectrum is much smaller than that of the envelope. As the dense spectrum contains ripples, in order to obtain its accurate dip for analysis, Gauss function is utilized again to fit a section of transmission spectrum with 3 nm wavelength range, and then, dip2 is obtained. In order to obtain a relative larger dynamic measurement range and more accurate wavelength shift measurement, we choose the resonant dips around 1550 nm and with highest extinction ratio as dip1 and dip2. As we can see from the picture, dip2 is much more sensitive than dip1 with external RI variation.

By heating the sucrose solution, representative interference spectrums at temperature of 35 °C and 40 °C are obtained and presented in Fig. 6. When temperature goes up, dip1 slightly move to longer wavelength while dip2 moves to shorter wavelength with high sensitivity. It should be noticed that the extinction ratio of the dense interference spectrum in temperature sensing is lower than that in RI sensing, which could attribute to the inhomogeneous

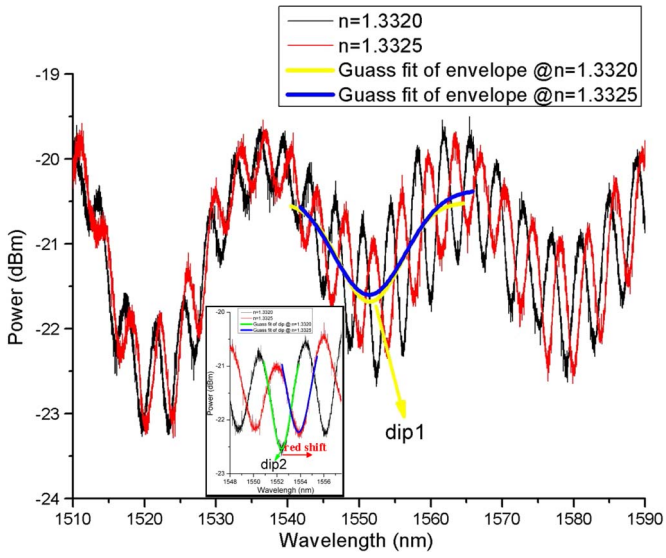

Fig. 5. Transmission spectrums in ambient RI of 1.3320 and 1.3325. (Inset) Enlarged spectrums with wavelength ranging from 1548 to 1557.5 nm.

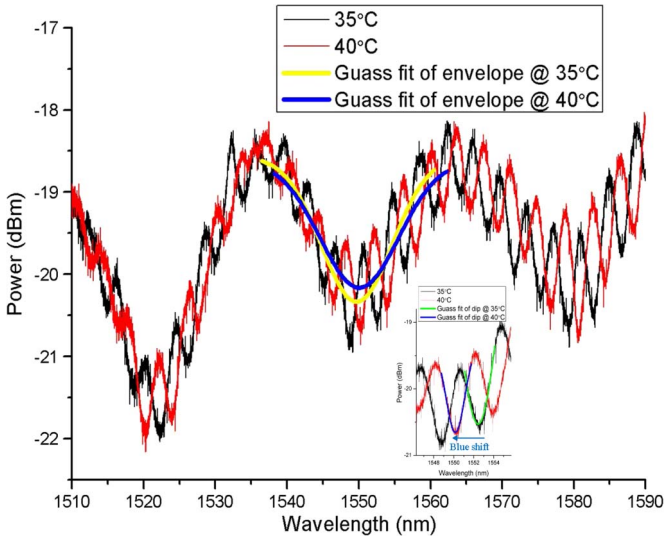

Fig. 6. Transmission spectrums at the temperature of 35 °C and 40 °C. (Inset) Enlarged spectrums with wavelength ranging from 1546.25 to 1555.75 nm.

temperature field. When the solution is localized heated rapidly, the temperature gradient will lead to the fluid flowing and then the micro-deformation of the fiber structure, and thus the energy attenuation of two modes in MMMF will be different from the initial state.

Fig. 7(a) shows the wavelength shift of dip1 and dip2 when RI increases from 1.3315 to 1.3350, with the sensitivities of −23.67 nm/RIU and 3820.23 nm/RIU, respectively. Although the measurement range in the experiment is relatively small due to the high sensitivity of dip2 it can be improved by increasing the spectrum interrogation scope. Meanwhile, It should be noticed that the RI sensitivity of dip2 is much higher than that of dip1, resulting from the weaker transverse light confinement in MMMF than that in SSMF. Further enhancement of the RI sensitivity of dip1 could be implemented by using thinned fiber (TF) instead of SSMF [14], [23]. Remarkably, the calculated sensitivity of dip2 at the external RI of 1.3320 based on (3) is 4145.5 nm/RIU, which agrees well with the experimental result.

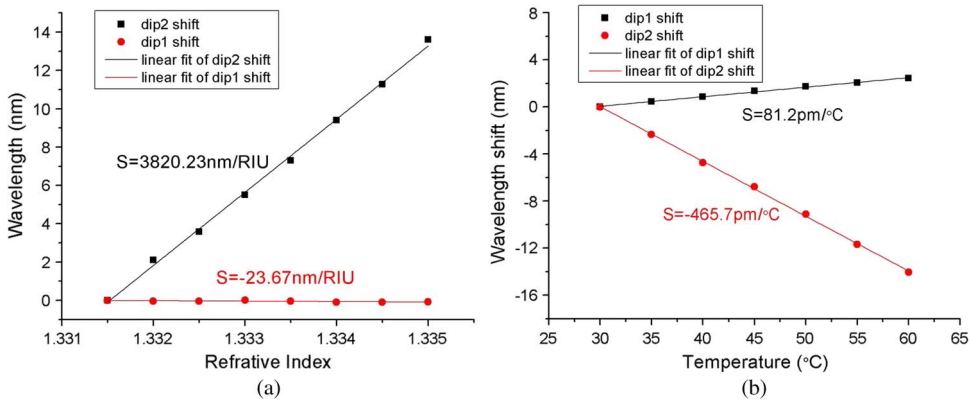

Fig. 7. (a) Wavelength shifts of dip1 and dip2 as a function of RI. (b) Wavelength shifts of dip1 and dip2 as a function of temperature.

Temperature sensing result is exhibited in Fig. 7(b), when temperature varies from 30 °C to 60 °C, dip1 shifts to longer wavelength while dip2 shifts to shorter wavelength with sensitivities of 81.2 pm/°C and −465.7 pm/°C, respectively. For the in-line MZI of the SSMF, the relationship between the wavelength shift of dip1 and temperature variation is actually the combined action of thermo-optic effect of sucrose solution and SSMF itself. Specifically, sucrose solution with thermo-optic coefficient of -1×10^{-4} RIU/°C will generate 2.367 pm wavelength shift per Celsius as one part temperature sensitivity of dip1. The other part of temperature sensitivity is caused by thermo-optic coefficients difference between the core and the cladding in SSMF. As a result, the two thermo-optic effects working together lead to red shift of dip1 with sensitivity of 81.2 pm/°C. For the other in-line MZI of MMMF, the theoretical sensitivity could be calculated as −428.5 pm/°C at SRI of 1.3310 according to (4), which also shows good coherence with the experimental sensitivity of −465.7 pm/°C.

From above, by tracking the wavelength shifts of dip1 and dip2 along with the RI and temperature variation, dual-parameters simultaneous measurement can be implemented by calculating the following function:

$$\begin{pmatrix} \Delta RI \\ \Delta T \end{pmatrix} = \begin{pmatrix} -23.67 \text{ nm/RIU} & 81.2 \text{ pm/°C} \\ 3820.23 \text{ nm/RIU} & -465.7 \text{ pm/°C} \end{pmatrix}^{-1} \begin{pmatrix} \Delta\lambda_{dip1} \\ \Delta\lambda_{dip2} \end{pmatrix} \tag{5}$$

where $\Delta\lambda_{dip1}$ and $\Delta\lambda_{dip2}$ are the wavelength shifts of dip1 and dip2, respectively. The big difference of RI sensitivities as well as that of temperature between dip1 and dip2 could provide a more accurate demodulation. Although the direct measurement range is limited by the narrow fringes, it can be greatly improved by the real-time wavelength tracking method [24].

4. Conclusion

We have proposed and demonstrated a microfiber based dual in-line MZI scheme to realize simultaneous measurement of RI and temperature. By tracking the wavelength shifts of certain resonant dips of the dual in-line MZI, RI sensitivities of −23.67 nm/RIU and 3820.23 nm/RIU, as well as temperature sensitivities of 81.19 pm/°C and −465.7 pm/°C for the two independent MZIs can be achieved. Such sensitivities with big difference between dip1 and dip2 could provide a more accurate demodulation of RI and temperature. Meanwhile, systematic theoretical analysis and simulation of the sensing performance have been done and the results demonstrate that the enhanced sensitivities of RI and temperature could be achieved by employing MMMF or SSMF with smaller diameter, as well as using liquid with higher thermo-optic coefficient and higher SRI. The sensor has great potential application in chemical and biological sensing fields due to its merits of multi-parameters measurement, compact structure, high sensitivity, low cost, and easy fabrication.

References

[1] H. F. Xuan, W. Jin, and M. Zhang, "CO2 laser induced long period grating in optical microfibers," *Opt. Exp.*, vol. 17, no. 24, pp. 21882–21890, Nov. 2009.

[2] G. Vienne *et al.*, "Demonstration of a reef knot microfiber resonator," *Opt. Exp.*, vol. 17, no. 8, pp. 6224–6229, Apr. 2009.

[3] P. F. Wang *et al.*, "Low-temperature sensitivity periodically tapered photonic crystal-fiber-based refractometer," *Opt. Lett.*, vol. 38, no. 19, pp. 3795–3798, Oct. 2013.

[4] G. S. Delgado, D. M. Hernandez, A. M. Rios, G. A. C. Sevilla, and J. Villatoro, "Optical microfiber mode interferometer for temperature-independent refractometric sensing," *Opt. Lett.*, vol. 37, no. 11, pp. 1974–1976, Jun. 2012.

[5] B. M. Felipe, H. O. Jonas, R. B. Claudecir, and C. M. B. Cordeiro, "D-microfibers," *J. Lightw. Technol.*, vol. 31, no. 16, pp. 2576–2761, Aug. 2013.

[6] J. H. Wo *et al.*, "Refractive index sensor using microfiber-based Mach–Zehnder interferometer," *Opt. Lett.*, vol. 37, no. 1, pp. 67–69, Jan. 2012.

[7] P. F. Wang *et al.*, "Fiber-tip high-temperature sensor based on multimode interference," *Opt. Lett.*, vol. 38, no. 22, pp. 4617–4620, Nov. 2013.

[8] Y. Wu, Y. J. Rao, Y. H. Chen, and Y. Gong, "Miniature fiber-optic temperature sensors based on silica/polymer microfiber knot resonators," *Opt. Exp.*, vol. 17, no. 20, pp. 18142–18147, Sep. 2009.

[9] Y. Xue *et al.*, "Ultrasensitive temperature sensor based on an isopropanol-sealed optical microfiber taper," *Opt. Lett.*, vol. 38, no. 8, pp. 1209–1211, Apr. 2013.

[10] J. J. Zhang *et al.*, "Microfiber Fabry–Perot interferometer for dual-parameter sensing," *J. Lightw. Technol.*, vol. 31, no. 10, pp. 1608–1615, May 2013.

[11] H. P. Luo, Q. Z. Sun, Z. L. Xu, D. M. Liu, and L. Zhang, "Simultaneous measurement of refractive index and temperature using multimode microfiber-based dual Mach–Zehnder interferometer," *Opt. Lett.*, vol. 39, no. 13, pp. 4049–4052, Jul. 2014.

[12] Y. Ran, L. Jin, L. P. Sun, J. Li, and B. O. Guan, "Bragg gratings in rectangular microfiber for temperature independent refractive index sensing," *Opt. Lett.*, vol. 37, no. 13, pp. 2649–2651, Jul. 2012.

[13] Y. Ran, L. Jin, L. P. Sun, J. Li, and B. O. Guan, "Temperature-compensated refractive-index sensing using a single Bragg grating in an abrupt fiber taper," *IEEE Photon. J.*, vol. 5, no. 2, Apr. 2013, Art. ID. 7100208.

[14] L. C. Li, L. Xia, Z. H. Xie, and D. M. Liu, "All-fiber Mach–Zehnder interferometers for sensing applications," *Opt. Exp.*, vol. 20, no. 10, pp. 11109–11120, May 2012.

[15] W. B. Ji, H. H. Liu, S. C. Tjin, K. K. Chow, and A. Lim, "Ultrahigh sensitivity refractive index sensor based on optical microfiber," *IEEE Photon. Technol. Lett.*, vol. 24, no. 20, pp. 1872–1874, Oct. 2012.

[16] A. J. Fielding and C. C. Davis, "Experimental observation of mode evolution in single-mode tapered optical fibers," *J. Lightw. Technol.*, vol. 17, no. 9, pp. 1649–1656, Sep. 1999.

[17] Y. Dai *et al.*, "Simultaneous measurement for liquid level and refractive index based on all-fiber modal interferometer," *J. Modern Opt.*, vol. 60, no. 6, pp. 496–502, Jun. 2014.

[18] L. V. Nguyen, D. Hwang, S. Moon, D. S. Moon, and Y. Chung, "High temperature fiber sensor with high sensitivity based on core diameter mismatch," *Opt. Exp.*, vol. 16, no. 15, pp. 11369–11375, Jul. 2008.

[19] J. H. Wo *et al.*, "Sensitivity-enhanced fiber optic temperature sensor with strain response suppression," *Opt. Fiber Technol.*, vol. 19, no. 4, pp. 289–292, Apr. 2013.

[20] L. M. Tong, J. Y. Lou, and E. Mazur, "Single-mode guiding properties of subwavelength-diameter silica and silicon wire waveguides," *Opt. Exp.*, vol. 12, no. 6, pp. 1025–1035, Mar. 2004.

[21] J. Li *et al.*, "Ultrasensitive refractive-index sensors based on rectangular silica microfibers," *Opt. Lett.*, vol. 36, no. 18, pp. 3593–3595, Sep. 2011.

[22] K. R. Sohn and K. T. Kim, "Thermo-optically tunable band-rejection filters using mechanically formed long-period fiber gratings," *Opt. Lett.*, vol. 30, no. 20, pp. 2688–2690, Oct. 2005.

[23] J. Yang *et al.*, "High sensitivity of taper-based Mach–Zehnder interferometer embedded in a thinned optical fiber for refractive index sensing," *Appl. Opt.*, vol. 50, no. 28, pp. 5503–5505, Oct. 2011.

[24] C. Gouveia *et al.*, "High resolution temperature independent refractive index measurement using differential white light interferometry," *Sensor Actuat B, Chem.* vol. 188, pp. 1212–1217, Aug. 2013.